Self-scheduled LPV controller synthesis for doubly-fed induction generators

Nguyen Tien, H.; Scherer, C.W.; Scherpen, J.M.A.

Published in:
Proceedings on Windpower 2007

Publication date:
2007

Self-scheduled LPV controller synthesis for doubly-fed induction generators

H. Nguyen Tien*, C. W. Scherer*, J. M. A. Scherpen**
*Delft Center for Systems and Control, Delft University of Technology, The Netherlands
**Faculty of Mathematics and Natural Sciences, University of Groningen, The Netherlands

***Abstract*— This paper presents a new current control design for doubly-fed induction generators in wind turbine systems, where the control is implemented on the rotor side. The mechanical angular speed of the rotor is considered as a time-varying parameter. A self-scheduled controller is then designed for the inner current loop in order to guarantee decoupling of torque and power factor, and to achieve high robust dynamic performance for all admissible trajectories of the rotor speed in the operating range. The closed loop system performance with the proposed controller is compared with a conventional control scheme. Performance and robustness of the controlled system are demonstrated via simulations.**

NOMENCLATURE

v_{sd}, v_{sq}	= d and q components of stator voltage;
v_{rd}, v_{rq}	= d and q components of rotor voltage;
i_{sd}, i_{sq}	= d and q components of stator current;
i_{rd}, i_{rq}	= d and q components of rotor current;
Ψ_{sd}, Ψ_{sq}	= stator flux components;
L_m	= mutual inductance;
L_s, L_r	= stator and rotor inductances;
R_s, R_r	= stator and rotor resistances;
$\sigma = 1 - \frac{L_m^2}{L_s L_r}$	= total linkage coefficient;
$T_s = \frac{L_s}{R_s}$	= time constant of stator;
$T_r = \frac{L_r}{R_s}$	= time constant of rotor;
ω_s	= stator electrical speed;
ω_r	= rotor electrical speed;
$\omega = \omega_s - \omega_r$	= rotor speed;
$a = \frac{1-\sigma}{\sigma}$	

I. INTRODUCTION

Doubly-fed induction machines (DFIMs) are often used as generators for variable speed wind turbines because of their advantages in comparison with other machines. The most important feature is that approximately 30% of the generator power is handled by power converters. Therefore, converters should be designed in a cost effective fashion.

In the regular configuration of variable speed wind turbines, the stator of DFIM is directly connected to the grid and the rotor is connected with two converters, one on the grid side, the so-called Grid Side Converter (GSC), and the other on the rotor side, the so-called Rotor Side Converter (RSC), coupled by a DC-voltage link as shown in Fig. 1.

The grid side converter is controlled to keep the DC-link voltage at a constant value and to supply an amount of required reactive power into the grid. The rotor side controller is used to control active and reactive powers on the stator side.

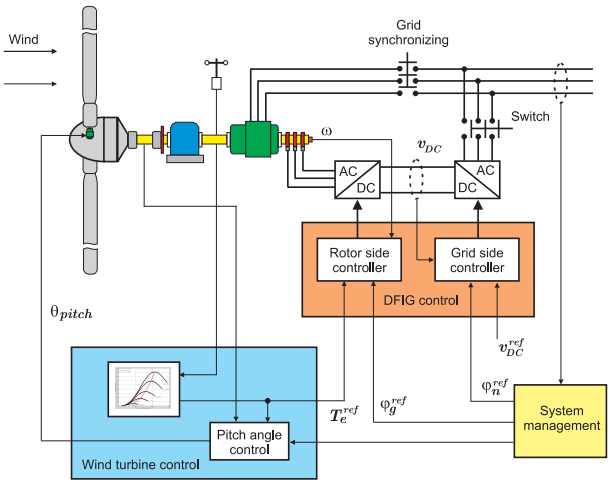

Fig. 1. Variable speed wind turbine system

II. MODELLING AND ANALYSIS OF DOUBLY-FED INDUCTION MACHINE

A. Machine modelling

In this paper, a dq reference frame, which is independent of the machine parameters and rotor speed measurement accuracy, is adopted. This reference frame has the d axis coinciding with the grid voltage vector [1]. In this reference frame, the DFIM equations can be written as

$$\begin{aligned}
\frac{di_{rd}}{dt} &= -\left(\frac{a+1}{T_r} + \frac{a}{T_s}\right) i_{rd} + (\omega_s - \omega) i_{rq} + \frac{a}{L_m T_s}\Psi_{sd} \\
&\quad - \frac{a\omega}{L_m}\Psi_{sq} - \frac{a}{L_m} v_{sd} + \frac{a+1}{L_r} v_{rd} \\
\frac{di_{rq}}{dt} &= (\omega - \omega_s) i_{rd} - \left(\frac{a+1}{T_r} + \frac{a}{T_s}\right) i_{rq} + \frac{a\omega}{L_m}\Psi_{sd} \\
&\quad + \frac{a}{L_m T_s}\Psi_{sq} - \frac{a}{L_m} v_{sq} + \frac{a+1}{L_r} v_{rq} \qquad (1) \\
\frac{d\Psi_{sd}}{dt} &= \frac{L_m}{T_s} i_{rd} - \frac{1}{T_s}\Psi_{sd} + \omega_s \Psi_{sq} + v_{sd} \\
\frac{d\Psi_{sq}}{dt} &= \frac{L_m}{T_s} i_{rq} - \omega_s \Psi_{sd} - \frac{1}{T_s}\Psi_{sq} + v_{sq}
\end{aligned}$$

Rewriting (1) in a compact form and in combination with the output equation leads to

$$\begin{pmatrix} \dot{x}_r \\ y_r \end{pmatrix} = \left(\begin{array}{c|cc} A_{rc}(\omega) & B_s & B_r \\ \hline C_{rc} & 0 & 0 \end{array}\right) \begin{pmatrix} x_r \\ v_s \\ v_r \end{pmatrix} \quad (2)$$

where $x_r = \begin{pmatrix} i_{rd} & i_{rq} & \Psi_{sd} & \Psi_{sq} \end{pmatrix}^T$; $v_s = \begin{pmatrix} v_{sd} & v_{sq} \end{pmatrix}^T$; $v_r = \begin{pmatrix} v_{rd} & v_{rq} \end{pmatrix}^T$; $y_r = i_r = \begin{pmatrix} i_{rd} & i_{rq} \end{pmatrix}^T$;

$$A_{rc}(\omega) = \begin{pmatrix} -\left(\frac{a+1}{T_r} + \frac{a}{T_s}\right) & \omega_s - \omega & \frac{a}{L_m T_s} & -\frac{a\omega}{L_m} \\ \omega - \omega_s & -\left(\frac{a+1}{T_r} + \frac{a}{T_s}\right) & \frac{a\omega}{L_m} & \frac{a}{L_m T_s} \\ \frac{L_m}{T_s} & 0 & -\frac{1}{T_s} & \omega_s \\ 0 & \frac{L_m}{T_s} & -\omega_s & -\frac{1}{T_s} \end{pmatrix};$$

$$B_s = \begin{pmatrix} -\frac{1-\sigma}{\sigma L_m} & 0 \\ 0 & -\frac{1-\sigma}{\sigma L_m} \\ 1 & 0 \\ 0 & 1 \end{pmatrix}; \quad B_r = \begin{pmatrix} \frac{1}{\sigma L_r} & 0 \\ 0 & \frac{1}{\sigma L_r} \\ 0 & 0 \\ 0 & 0 \end{pmatrix};$$

$$C_{rc} = \begin{pmatrix} 1 & 0 & 0 & 0 \\ 0 & 1 & 0 & 0 \end{pmatrix}.$$

B. Open loop analysis

Let us analyze the system (2) denoted by G_r.

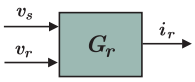

Fig. 2. The plant model

As illustrated in Fig. 2, the rotor voltages v_r are the control inputs, the controlled outputs are the rotor current i_r, while the stator voltages v_s can be considered as the input disturbances.

The frequency responses of the channels $v_s \rightarrow i_r$ can be seen in Fig. 3 and 4. The time response of the rotor currents with respect to the rotor voltages v_r and the stator voltages v_s for some values of ω in its operating range can be seen in Fig. 5.

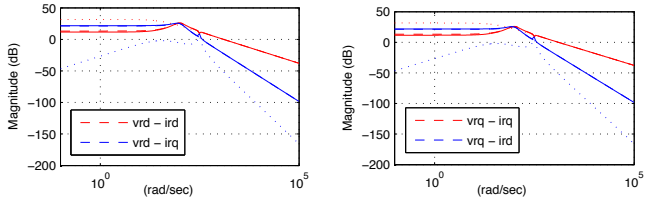

Fig. 3. Bode magnitude plot from the rotor voltages v_r to the rotor currents i_r. Dash lines: $\omega = 0.7\omega_s$, dotted line: $\omega = \omega_s$, and solid line: $\omega = 1.3\omega_s$

An analysis of the open-loop shows:

- Stator (gird) voltages can be considered as input disturbance.
- The bandwidth is close to the excitation frequency of stator voltages [2], [3].
- Because of the magnetic coupling between stator and rotor, variations of grid voltages result in oscillations in rotor currents.

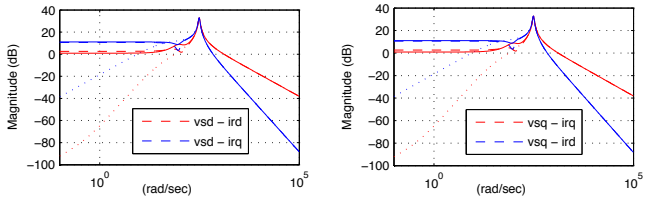

Fig. 4. Bode magnitude plot from the stator voltages v_s to the rotor currents i_r. Dash lines: $\omega = 0.7\omega_s$, dotted line: $\omega = \omega_s$, and solid line: $\omega = 1.3\omega_s$

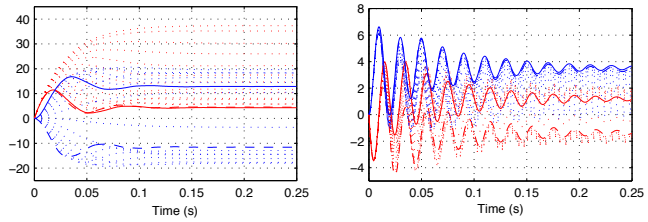

Fig. 5. Open loop time response of the rotor currents i_r with respect to the rotor voltages v_r (left) and the stator voltages v_s (right) for 15 values of ω in the range of $[0.7\omega_s, 1.3\omega_s]$

- In the normal operation the stator voltage v_s is assumed to be a constant. However, in some specific cases such as grid faults, the sag in the grid voltage will results in a significant influence on the performance of the system.

III. Control of DFIM in Wind Turbine Systems

A. Control structure

The total control structure of DFIM in a Wind Energy Conversion System (WECS) is shown in Fig. 6. Here two current controllers are designed for the rotor and grid side converters respectively. However, in this paper, only the control structure on the rotor side with two loops as shown in Fig. 7 is discussed. The inner loop in Fig. 7 with controller K_{rc} is called the rotor current control loop. The design goal of the rotor current controller K_{rc} is to achieve high dynamic performance and robust tracking of the rotor currents. The outer loop with controller K_g is called the electrical torque control loop used for tracking the optimal values of electrical torque T_e^{ref} and power factor φ_g^{ref}. In Fig. 7, G_r represents the plant according to equations (2); y_g is the controlled output that is estimated from the outputs of the plant. Based on the actual measured values of the wind speeds and the characteristics of each particular wind turbine, the main control station will track the optimum torque from a look-up table and use it as the reference value for the power electronics control stage.

The electrical torque of the DFIM on the dq reference frame aligned to the stator voltage, i.e. $\Psi_{sd} = 0$, can be computed by

$$T_e = -\frac{3}{2} p \frac{L_m}{L_s} \Psi_{sq} i_{rd}. \quad (3)$$

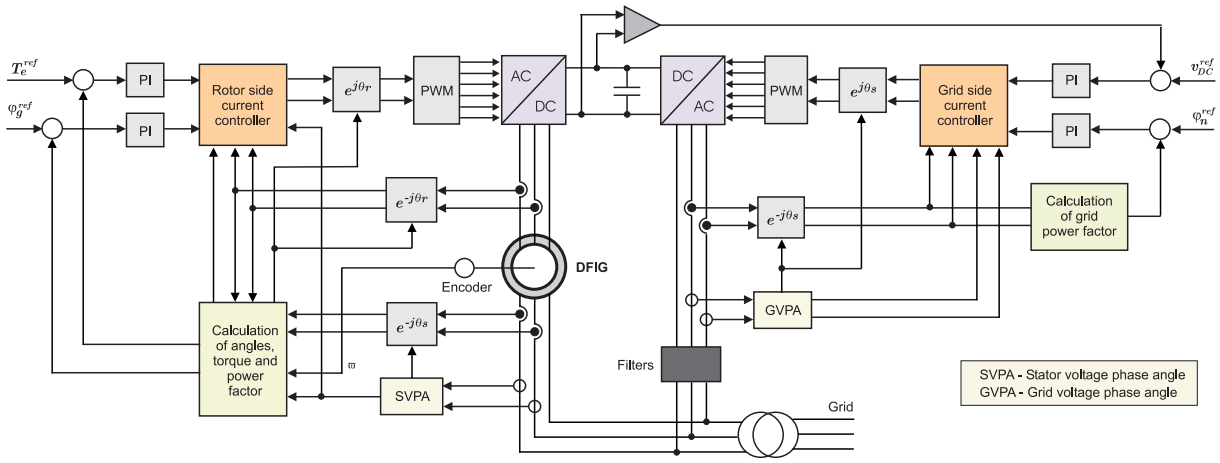

Fig. 6. The total control structure of DFIM

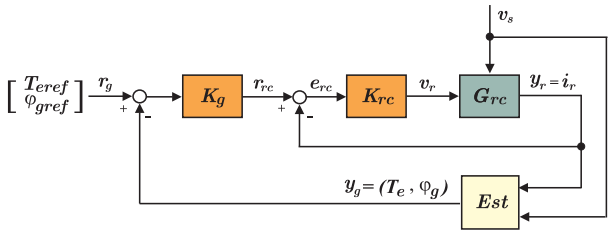

Fig. 7. Rotor side current control loop

On the other hand, controlling the reactive power can be implemented by regulating the power factor φ. This factor can be computed as follows:

$$\varphi = arcsin \frac{i_{sq}}{\sqrt{i_{sd}^2 + i_{sq}^2}}. \tag{4}$$

The equations (3) and (4) show that the torque and power factor of the DFIM can be regulated via the components of the rotor currents i_{rd} and i_{rq}.

The essential common features of the conventional design methods [4], [5], [6], [7], [8] to design the current controller K_{rc} are:

- The vector control technique [9] is used which allows one to achieve decoupled control of active and reactive powers in both generator and motor operations.
- The difficulties of the nonlinear dynamics of DFIG are not taken into account, i.e. the model of the machine is linearized and it is assumed that both the machine parameters required by the control algorithm and the grid voltage are precisely known.
- The closed-loop behavior is highly sensitive to a change of the operating conditions and/or parameters.

In this paper, the rotor current controller is designed based on the linear parameter varying (LPV) systems approach [10], [11], [12]. In this approach, the rotor mechanical angular speed ω in (1) is considered as a time varying parameter or, in other words, as a scheduling variable. This particular choice is motivated by the fact that ω, which causes the system to be nonlinear, can be measured online. Then, a self-scheduled controller is designed for the inner current control loop in order to achieve high robust dynamic performance for all admissible trajectories of the rotor speed in the operating range.

B. LPV representation of DFIM model

In fact, the rotor mechanical angular speed varies by $\pm 30\%$ around the synchronous speed ω_s. Therefore, with $-1 \leq \delta_\omega \leq 1$ and $p_\omega = 0.3$, the mechanical angular speed can be expressed as $\omega = \omega_s(1 + p_\omega \delta_\omega)$. Thus (1) now becomes affinely parameter dependent and can be rewritten as

$$\dot{x}_r = (A_{rs} + \delta_\omega A_{r\omega})\, x_r + B_s v_s + B_r v_r \tag{5}$$

where $A_{rs}, A_{r\omega}$ are matrices defined by

$$A_{rs} = \begin{pmatrix} -\left(\frac{a+1}{T_r} + \frac{a}{T_s}\right) & 0 & \frac{a}{L_m T_s} & -\frac{a\omega_s}{L_m} \\ 0 & -\left(\frac{a+1}{T_r} + \frac{a}{T_s}\right) & \frac{a\omega_s}{L_m} & \frac{a}{L_m T_s} \\ \frac{L_m}{T_s} & 0 & -\frac{1}{T_s} & \omega_s \\ 0 & \frac{L_m}{T_s} & -\omega_s & -\frac{1}{T_s} \end{pmatrix};$$

$$A_{r\omega} = \begin{pmatrix} 0 & -\omega_s p_\omega & 0 & -\frac{a\omega_s p_\omega}{L_m} \\ \omega_s p_\omega & 0 & \frac{a\omega_s p_\omega}{L_m} & 0 \\ 0 & 0 & 0 & 0 \\ 0 & 0 & 0 & 0 \end{pmatrix}.$$

With $\Delta_\omega = \begin{pmatrix} \delta_\omega & 0 \\ 0 & \delta_\omega \end{pmatrix}$, the system (5) can be rewritten as follows:

$$\begin{pmatrix} \dot{x}_r \\ \hline y_r \\ \hline z_\omega \end{pmatrix} = G_{rc} \begin{pmatrix} x_r \\ \hline v_s \\ v_r \\ \hline w_\omega \end{pmatrix}, \quad w_\omega = \Delta_\omega z_\omega \tag{6}$$

where

$$G_{rc} = \left(\begin{array}{c|ccc} A_{rs} & B_s & B_r & B_{r\omega} \\ \hline C_{rc} & 0 & 0 & 0 \\ \hline C_{r\omega} & 0 & 0 & 0 \end{array}\right);$$

$$C_{r\omega} = \begin{pmatrix} 0 & -\omega_s p_\omega & 0 & -\frac{a\omega_s p_\omega}{L_m} \\ \omega_s p_\omega & 0 & \frac{a\omega_s p_\omega}{L_m} & 0 \end{pmatrix};$$

$$B_{r\omega} = \begin{pmatrix} 1 & 0 & 0 & 0 \\ 0 & 1 & 0 & 0 \end{pmatrix}^T; \quad y_r = \begin{pmatrix} i_{rd} & i_{rq} \end{pmatrix}^T.$$

C. H_∞ control of the LPV system

A mixed sensitivity T/S loop shaping H_∞ optimization [13] is proposed for the rotor current control loop (see Figure 7). The external control inputs w_{rc} consist of stator voltages and reference rotor currents $w_{rc} = \begin{pmatrix} v_{sd} & v_{sq} & i_{rd}^{ref} & i_{rq}^{ref} \end{pmatrix}^T$. The controller outputs are $v_r = \begin{pmatrix} v_{rd} & v_{rq} \end{pmatrix}^T$. The controller inputs or tracking errors are $e_r = \begin{pmatrix} e_{rcd} & e_{rcq} \end{pmatrix}^T = \begin{pmatrix} i_{rd}^{ref} - i_{rd} & i_{rq}^{ref} - i_{rq} \end{pmatrix}^T$. The measured outputs are $y_r = \begin{pmatrix} i_{rd} & i_{rq} \end{pmatrix}^T$. The sensitivity function is $S_{rc} = (I + G_{rc}K_{rc})^{-1}$ and the complementary sensitivity function is $T_{rc} \triangleq I - S_{rc}$.

The interconnection of the system used for synthesis is shown in Figure 8. The weighting function

$$W_{rs} = \text{diag}\,(W_{rsd}, W_{rsq}) = \begin{pmatrix} \frac{0.198s+3000}{s+0.003} & 0 \\ 0 & \frac{0.1739s+3000}{s+0.003} \end{pmatrix}$$

is the low-pass filter used to shape the sensitivity for tracking. The weighting function

$$W_{rt} = \text{diag}\,(W_{rtd}, W_{rtq}) = \begin{pmatrix} \frac{s+0.0003}{0.01905s+3000} & 0 \\ 0 & \frac{s+0.0003}{0.01538s+3000} \end{pmatrix}$$

is the high-pass filter used to shape the complementary sensitivity function to guarantee robustness against high frequency un-modelled dynamics.

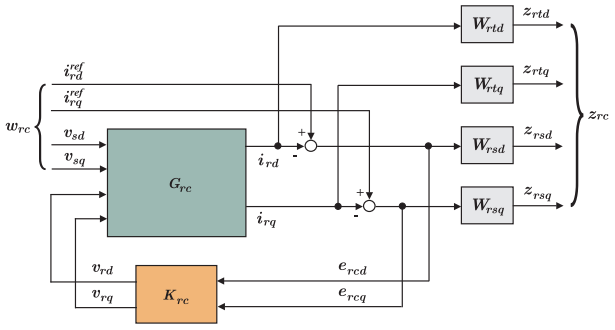

Fig. 8. The interconnection of the system

The H_∞ control problem is to find a stabilizing LTI controller $K_{rc}(\omega)$ at fixed frozen values of ω such that the H_∞-norm of the channel $w_{rc} \rightarrow z_{rc}$ is smaller than a specified bound γ, namely

$$\left\| \begin{matrix} W_{rt}T_{rc} \\ W_{rs}S_{rc} \end{matrix} \right\|_\infty < \gamma.$$

D. Synthesis of gain-scheduled current controller

The gain-scheduled controller synthesis is similar to the classical H_∞ synthesis, but both the plant and the controller are now LPV systems. The optimization problem is to find a stabilizing controller $K_{rc}(\omega)$ such that the $\mathcal{L}_2$-gain of the channel $w_{rc} \rightarrow z_{rc}$ is smaller than γ for all trajectories of $\omega(t) \in [\omega_{min}, \omega_{max}] = [(1-p_\omega)\omega_s, (1+p_\omega)\omega_s]$.

We employ the Linear Matrix Inequality (LMI) Control Toolbox in Matlab [14] in order to compute the vertex controllers

$$K_{rc1} = \begin{pmatrix} A_{Krc1} & B_{Krc1} \\ C_{Krc1} & D_{Krc1} \end{pmatrix}, \quad K_{rc2} = \begin{pmatrix} A_{Krc2} & B_{Krc2} \\ C_{Krc2} & D_{Krc2} \end{pmatrix}$$

in a polytopic controller description. Then the controller is implemented as follows: for a value $\omega(t)$ measured at time t, we use

$$K_{rc}(t) = \frac{\delta_w^{max} - p(t)}{\delta_w^{max} - \delta_w^{min}} K_{rc1} + \frac{p(t) - \delta_w^{min}}{\delta_w^{max} - \delta_w^{min}} K_{rc2}$$

with $p(t) = \frac{\omega(t) - \omega_s}{\omega_s p_w}$ for simulating the controller dynamics.

The Bode plots of the closed-loop system with the LPV controller in Fig. 9, 10, and 11 show that the designed controller maintains the performance requirements specified by W_{rt} and W_{rs} for some frozen rotor speeds in its variation range.

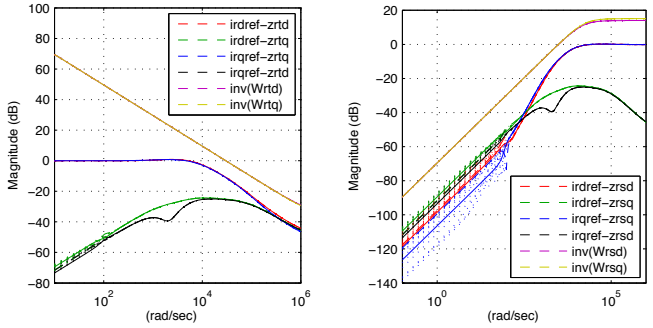

Fig. 9. Close-loop frequency response of the complementary sensitivity function T_{rc} with inverted weighting function W_{rt} (left) and sensitivity function S_{rc} with inverted weighting function W_{rs} (right) for 7 values of ω in the range of $[0.7\omega_s, 1.3\omega_s]$

IV. Simulations

A. Performance of the system with step changes of electrical torque and power factor

Fig. 12 shows the performance of the controlled system depicted in Fig. 7 tested with step changes of the reference

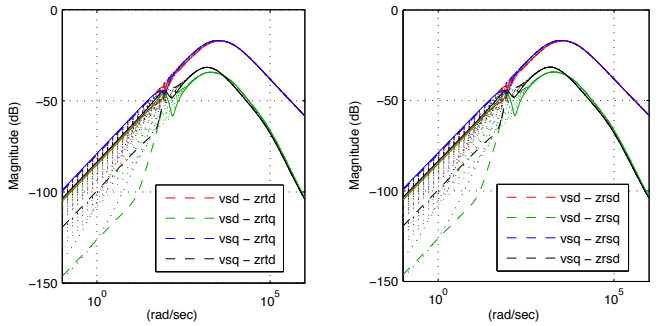

Fig. 10. Bode magnitude plots of the effects of the stator voltages v_s to the rotor currents i_r (left) and control errors e_r (right) for 7 values of ω in the range of $[0.7\omega_s, 1.3\omega_s]$

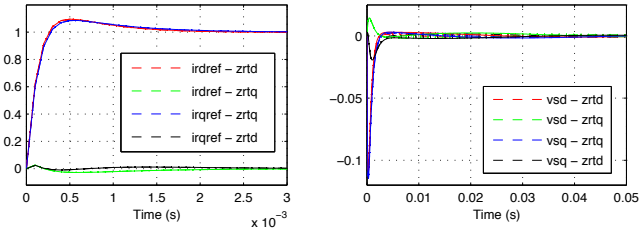

Fig. 11. Close-loop time responses of the rotor currents i_r with respect to the references $i_r^{ref} = \begin{pmatrix} i_{rd}^{ref} & i_{rq}^{ref} \end{pmatrix}^T$ (left) and the stator voltages v_s (right) for 7 values of ω in the range of $[0.7\omega_s, 1.3\omega_s]$

values for the electrical torque T_e and the power factor $sin\varphi$. The initial value of the torque is -500Nm. Then it increases to -1500Nm at time 3s. Finally, it decreases to -1250Nm at time 7s. Meanwhile, the set value of φ increases from the initial value of 0.05 to 0.3 at the time 2s, and then it decreases to 0.1 at the time 6s. We see from Fig. 12 that the electrical torque T_e and the power factor $sin\varphi$ accurately track their reference values. The decoupling effect of the controller can be extracted from the fact that torque control is achieved by controlling the d-component, while power factor control is achieved by controlling the q-component of the rotor currents.

B. Performance of the system with stator voltage dip

When the grid undergoes a fault, the sag in the grid voltage will result in an increase of the current in the stator windings of the DFIM. Because of the magnetic coupling between stator and rotor, this current will also flow into the rotor circuit and the power converter leading to the destruction of the converter if nothing is done to protect it. On the other hand, the study in [7] shows that the dynamics of the DFIM has poorly damped poles in the transfer function of an LTI model of the machine. This will cause oscillations in the flux if the DFIM is affected by grid disturbances. After such disturbances, an increased rotor voltage will be needed to control the rotor currents. When this required voltage exceeds the voltage limit of the converter, it is not possible any longer to control the current as desired [15]. Therefore, the control system should maintain the

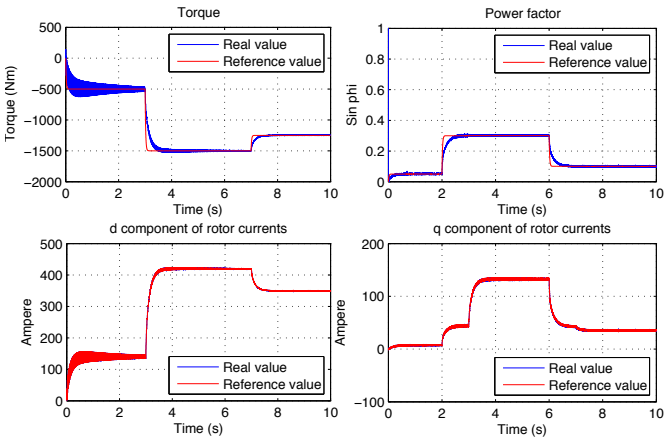

Fig. 12. The performance of the system with step changes

operation and reduce oscillations as much as possible during grid voltage faults.

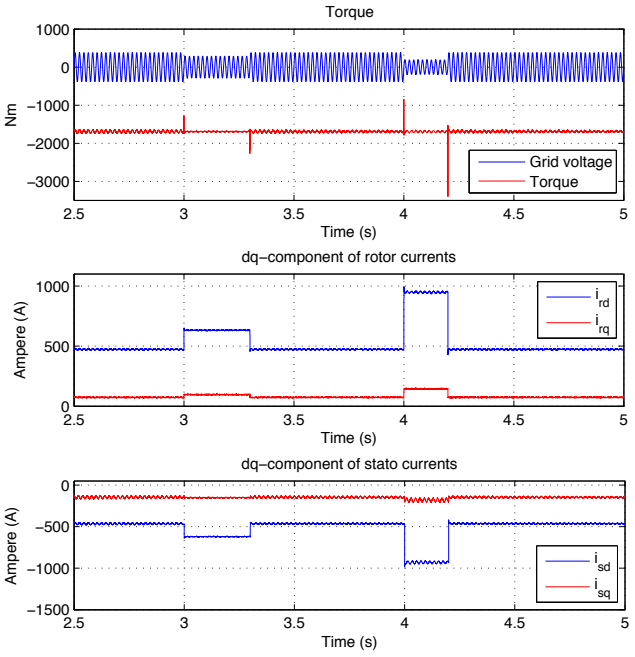

Fig. 13. The performance of the system when grid voltage is faulty

In Fig. 13, the grid voltage was dropped down to 25% of the normal voltage. This phenomenon occurred in a period of 300 msec before it recovered to its rated value. After that, the grid voltage was once again dropped to 50% of the rated voltage during 200 msec. The graphs show that the oscillations of torque and currents were remarkably dampened at the grid voltage fault time.

More results compared in two complete simulation models, one based on a conventional control scheme called dead-beat control (similar to that in [16]) and the other based on the described LPV framework, can be found in the poster. The

details of LPV controller synthesis for affinely parameter-dependent systems, the resulting performance of the controlled system with respect to the time-varying parameter, and robust performance of self-scheduled LPV control of DFIM in comparison with the dead-beat controller under parameter changes as well as grid voltage faults will be given in a future paper.

V. Conclusion

This paper presents self-scheduled LPV controller synthesis for the doubly-fed induction generator in a variable speed wind turbine system. The characteristics of the open-loop of the plant as well as the closed-loop of the controlled system were analyzed. The LPV framework was based on considering the online measurable rotor mechanical angular speed as a time-varying parameter. Hence the designed controller achieves robust tracking for the rotor currents of the inner loop for all trajectories of the rotor speed over its operating range. As a result, one also achieves tracking of optimal values of the electrical torque and the power factor in the outer loop of the rotor side. Furthermore, the simulation results show that performance of the closed-loop system was confirmed during the grid faults.

VI. Acknowledgments

The authors would like to thank the Vietnamese Government for the financial support through the project 322.

References

[1] S. Peresada, A. Tilli, and A. Tonielli. Power control of a doubly fed induction machine via output feedback. *Control Engineering Practice*, 12:41 – 57, 2004.

[2] A. Petersson, L. Harnefors, and T. Thiringer. Evaluation of current control methods for wind turbines using doubly fed induction machines. *IEEE transactions on Power Electronics*, 20:227–235, 2005.

[3] L. Congwei, W. Haiqing, S. Xudong, and L. Fahai. Research of stability of double fed induction motor vector controlsystem. *International Conference on Electrical Machines and Systems, Shenyang, China*, 2:1203–1206, Aug 2001.

[4] A. Tapia, G. Tapia, and J. X. Ostolaza. Reactive power control of wind farms for voltage control applications. *Renewable Energy*, 29:377–392, 2004.

[5] B. Hopfensperger, D.J. Atkinson, and R. A. Lakin. Stator flux oriented control of a double-fed induction machine with and without position encoder. *IEE Proc.-Electr. Power Appl.*, 147:241–250, 2000.

[6] R. Pena, J. C. Clare, and G. M. Asher. Doubly fed induction generator using back-to-back pwm converters and its application to variable speed windenergy generator. *IEE Proceedings on Electric Power Applications*, 143:231–241, 1996.

[7] A. Petersson. *Analysis, Modeling and Control of Doubly-Fed Induction Generators for Wind Turbines*. PhD thesis, Chalmers University of Technology, 2003.

[8] A. Tapia, G. Tapia, J. X. Ostolaza, and J. R. Saenz. Modeling and control of a wind turbine driven doubly fed induction generator. *IEEE Transactions on Energy Conversion*, 18:194– 204, June 2003.

[9] W. Leonhard. *Control of electrical drives*. Springer, 1996.

[10] S. Bennani, D. M. C. Willemsen, and C. W. Scherer. Robust LPV control with bounded parameter rates. *AIAA Guidance, Navigation, and Control Conference, New Orleans, LA*, pages 1080–1089, Aug. 11-13, 1997.

[11] P. Apkarian and R.J. Adams. Advanced gain-scheduling techniques for uncertain systems. *IEEE Transactions on Control Systems Technology*, 6:21 – 32, Jan. 1998.

[12] P. Apkarian, P. Gahinet, and G. Becker. Self-scheduled H_∞ control of linear parameter varying systems: a design example. *Automatica*, 31:1251–1261, 1995.

[13] S. Skogestad and I. Postlethwaite. *Multivariable feedback control - Analysis and design*. John Wiley & Sons, 1996.

[14] P. Gahinet, A. Nemirovski, A. J. Laub, and M. Chilali. *LMI Control Toolbox for use with Matlab*, volume 1. The Mathworks, 1995.

[15] M. Johan and S. W. H. de Haan. Ridethrough of wind turbines with doubly-fed induction generator during a voltage dip. *IEEE Transactions on energy conversion*, 20:435–441, Jun 2005.

[16] N. P. Quang, A. Dittrich, and A. Thieme. Doubly-fed induction machine as generator: control algorithms with decoupling of torque and power factor. *Electrical Engineering (Archiv fur Elektrotechnik)*, 80:325–335, 1997.